

ANALYSIS OF MICROSTRUCTURE FEATURES OF THE WINTER HAZE AEROSOL USING THE RESULTS OF OPTICAL MEASUREMENT DATA INVERSION

E.V. Makienko, Yu.A. Pkhalagov, R.F. Rakhimov, V.N. Uzhegov, and N.N. Shchelkanov

*Institute of Atmospheric Optics,
Siberian Branch of the Russian Academy of Sciences, Tomsk
Received December 29, 1994*

We analyze some peculiar features in aerosol particle size distributions characteristic of winter season based on inverting experimental data on spectral behavior of the aerosol extinction coefficient in the spectral range from 0.44 to 3.9 μm obtained in the ground atmospheric layer along a horizontal path. Some estimates of the main integral characteristics of the aerosol microstructure averaged over the period of observations are given in the paper for accumulative and coarse aerosol fractions. These parameters are classified with respect to the meteorological visual range.

Information on seasonal variability of the particle size distribution, concentration, and optical characteristics, both regional and local, is important for studies of the influence of neighbour regions on the formation of the fields of industrial aerosol in the process of long-range transfer of air masses. The problem of studying the aerosol as a factor of weather formation and many other applied problems of atmospheric optics need for such an information as well.

In Siberia, an extended series of daily winter observations of spectral atmospheric transmission in the visible and IR was first undertaken in Tomsk in December, 1992 (Ref. 1). The measurements have been conducted along a 1 km-long horizontal path using an automated multispectral meter of atmospheric spectral transmission.² A total of 199 measurements of spectral coefficient of aerosol extinction, $\beta_\varepsilon(\lambda)$, were performed in 22 spectral bands between 0.44 and 12.4 μm wavelengths. Characteristics of aerosol extinction for the visible and IR radiation were investigated in various types of optical weather,¹ and, through solving an inverse problem, the dynamics of particle size spectrum was studied for the case of optically dense winter haze during its formation and evolution.³ In this paper we continue these studies and analyze specific features of aerosol microstructure in winter inverted from the averaged optical characteristics of hazes of different densities.

Having the spectral dependences of aerosol extinction coefficients $\beta_\varepsilon(\lambda)$ obtained, the size distribution of particle cross sections, $s(r)$, is found by solving the system of equation of the form

$$\int_{R_1}^{R_2} K_\varepsilon(r, \lambda_i) s(r) dr = \beta_\varepsilon(\lambda_i), \quad (1)$$

where r is the particle radius, $K_\varepsilon(r, \lambda_i)$ is the extinction efficiency factor at the wavelength λ_i dependent on the complex refractive index, $m - i\kappa$, of the particulate matter. Equation (1) was inverted using a regularization algorithm,⁴ in which the vector of approximate solution, s^* , characterizing the function $s(r)$, was found by minimization of the smoothing functional in k -dimensional vector space. According to Tikhonov regularization, the functional T_α is written as

$$T_\alpha(s) = \sum_{i=1}^n \left(\sum_{l=1}^k Q_{\varepsilon,il} s_l - \beta_{\varepsilon,i} \right)^2 + \alpha \Omega(s), \quad (2)$$

where s_l are the components of the vector-solution; $Q_{\varepsilon,il}$ are the elements of matrix calculated using quadrature formulas⁵ on a fixed node grid, r_l ($l = 1, 2, \dots, k$) and λ_i ($i = 1, 2, \dots, n$), for the extinction efficiency factor in Eq. (1); α is the regularization parameter; and, $\Omega(s)$ is the smoothing functional, the form of which is determined by specific limitations on the solution sought.⁶ The value of the parameter α was chosen by trial and error method⁶ in accordance with the level of measurement error. The lower boundary R_1 of the solution domain, whose precise value has no appreciable impact on the value of $\beta_\varepsilon(\lambda)$ calculated from Eq. (1) was chosen to be 0.05 μm . The upper boundary of the size spectrum, R_2 , was estimated following the recommendations in Ref. 7 as

$$(R_2)^{-1} \int_{R_2}^{R_1} K_\varepsilon(\lambda_{\max}, r) dr = K_m \frac{\beta(\lambda_{\max})}{\beta_{\max}}, \quad (3)$$

where $K_m = \beta_{\max}/S$ is the polydispersion extinction efficiency factor calculated for the maximum in the

$$S = \int_{R_2}^{R_1} s(r) dr.$$

Thus obtained value of R_2 was then adjusted by an iterative technique from Ref. 8. For $\lambda_n = 3.9 \mu\text{m}$, the R_2 estimates for different $\beta_\epsilon(\lambda)$ samples ranged from 4.3 to 4.7 μm .

The spectral dependences $\beta_\epsilon(\lambda)$ for ten wavelengths between 0.44 and 3.9 μm are shown in Fig. 1, averaged for different levels of meteorological visual range, S_m . The inversion of the data is illustrated in Fig. 2, for the complex refractive index chosen according to the model from Ref. 9 ($m = 1.36 - i0.001$ for visible range), and considering that the relative air humidity exceeded 90% in the majority of observations.

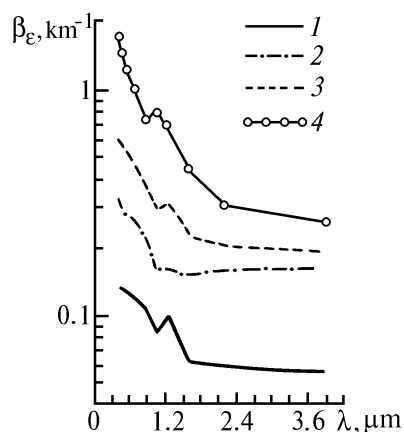


FIG. 1. Measured spectral behaviors of aerosol extinction coefficient averaged over December, 1992 for different values of meteorological visual range S_m : $S_m > 20 \text{ km}$ (1), $10 \text{ km} < S_m < 20 \text{ km}$ (2), $5 \text{ km} < S_m < 10 \text{ km}$ (3), and $S_m < 5 \text{ km}$ (4).

Typically, all distributions $s(r)$ reconstructed clearly demonstrate the existence of two aerosol fractions, the accumulative fraction of submicron particles, and the coarse fraction with the modal radius r_s of 2.6 to 2.9 μm . That is clearly seen in $s(r)$ -curves in Fig. 2, for $S_m > 20 \text{ km}$ and for $S_m < 5 \text{ km}$. In two other optical situations in the atmosphere, when $20 \text{ km} > S_m > 10 \text{ km}$ and $10 \text{ km} > S_m > 5 \text{ km}$, the distributions $s(r)$ contain distinct medium-sized fraction of particles in the size range of 0.8 to 2.5 μm , which seems to originate from urban industrial pollution.³ Under background conditions ($S_m > 20 \text{ km}$) and in the strongly turbid atmosphere ($S_m < 5 \text{ km}$), this fraction contributes relatively insignificantly, but enough to be observed

even in the situations presented in Fig. 1. Changing the slope of distribution $s(r)$ for $r > 0.8 \mu\text{m}$, the medium-sized fraction tends to mask the boundary between the two main aerosol fractions, shifting it toward larger values.

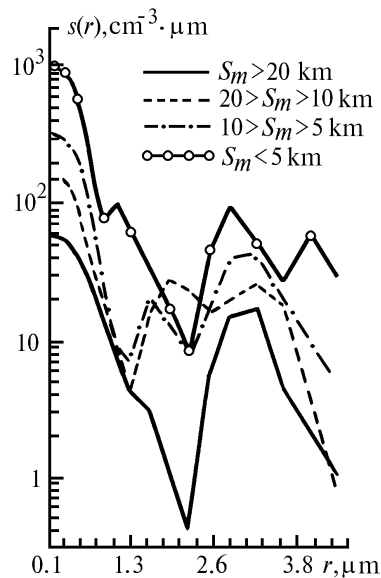


FIG. 2. Particle geometrical cross section distributions obtained by inverting the data presented in Fig. 1.

The above noted details in aerosol microstructure, revealed by solving the inverse problem, are clearly seen in Fig. 3, which compares distribution $s(r)$, reconstructed from data averaged for December, 1992 (curve 2), to various model aerosol distributions based on *in situ* measurements of aerosol concentration in the atmosphere.

The model distributions in Fig. 3 for urban and background aerosols (curves 1 and 3, respectively) were constructed based on data from Ref. 10 for the integral microstructure characteristics, by assuming lognormal particle size distribution for each aerosol fraction.

Another background aerosol model in Fig. 3 (curve 4) is that developed at IAO SB RAS¹¹ by analyzing and summarizing *in situ* microphysical data available. A comparison between models 3 and 4 shows the spread in theoretical representation of the aerosol microstructure being based on different initial data.

As is clear from Fig. 3, the separation into the coarse and medium-sized aerosol fractions and the evolution of the coarse fraction within a narrow range of particle size represent the key difference between the distributions $s(r)$, reconstructed from optical data, and the model results. Seemingly, the microstructure features of medium-sized aerosol are related to particular local conditions, while the existing right-hand cutoff in the coarse fraction spectrum occurs most likely due to depleted blowing out of particulates larger than 5 μm in radius from the surface in winter season.

The models illustrated in Fig. 3 (Refs. 10 and 11) are unable to reproduce variation of particle size spectrum throughout a year. Because of specific character of the winter season (snow-covered underlying surface, negative air temperature), it is interesting to compare the data for winter conditions. Such data are presented in Fig. 4, showing one typical sample of the distribution $s(r)$ measured by a photoelectric counter A3-5 in winter (in December, 1992 in Tomsk); the data were kindly provided by Dr. B.D. Belan.

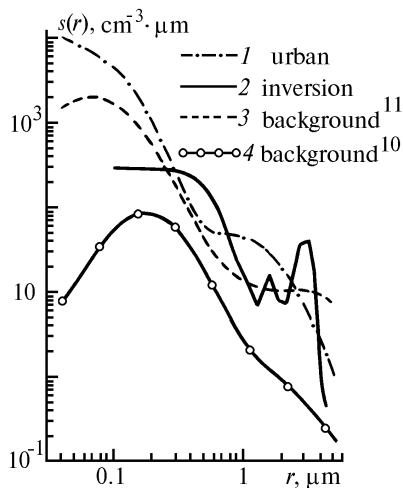


FIG. 3. Boundary-layer aerosol models^{10,11} compared to distribution $s(r)$ retrieved by inverting optical data averaged over the period of measurements (December, 1992). Data from Ref. 10 (1 and 4), data from Ref. 11 (3), and results of the solution of the inverse problem (2).

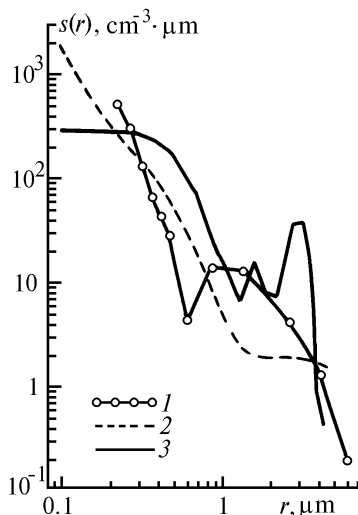


FIG. 4. Particle cross section distributions for winter season. Photoelectric counter (December, 1992, Tomsk) (1), model from Ref. 12 (2), and inversion of optical data (3).

As is seen from Fig. 4, the photoelectric counter does separate accumulative aerosol fraction from the medium-sized one, while significantly underestimating the concentration of the coarse fraction relative to values inverted from optical data. This is quite natural because of the essentially different bulks of data averaged in these two cases. The same remark applies to the distribution $s(r)$ (curve 2) reconstructed from the model data on particle size distribution in winter, which were derived in Ref. 12 from measurements in rural Central Povolzhie using a photoelectric counter "Kvant".

The steep slope should be noted in the model function $s(r)$ (curve 2) for particles with $r < 0.2 \mu\text{m}$, whose size distribution for winter season, as shown in Ref. 12, is best fit by a power-law $n(r) = Cr^{-\nu}$ with the value $\nu = 5$ (the standard literature value is $\nu = 3$). Relatively high concentration of small particles over snow cover is argued in Ref. 12 to be supposedly due to a decreased connective-turbulent air exchange in winter, and to reduced blowing off of particles with $r \geq 7 \mu\text{m}$ from the surface.

Our estimate of ν for $r < 0.3 \mu\text{m}$ is approximately four. It is important, therefore, to note that, with the photometric devices typically operating down to $\lambda_1 = 0.44 \mu\text{m}$, the measured optical characteristics badly represent particles with radii $r < 0.15 \mu\text{m}$. A practical consequence for the measurement result interpretation, as a numerical analysis shows, is a 20 to 30% underestimation of $S(r < 0.15 \mu\text{m})$, for a 10% error in optical measurements. For $S(r > 0.15 \mu\text{m})$, the retrieval error is within the uncertainty of the initial data.

The distribution $s(r)$, as well as the corresponding total geometrical cross section, well suit the study of the effect of changing microstructure on the atmospheric optical characteristics. Even more convenient in some applications, such as atmospheric aerosol pollutions, is to use the particle volume distribution $v(r) = (4/3)\pi r^3 n(r)$, together with the corresponding total particle volume V per cubic cm of air. With these, it is possible to estimate mass concentration of particles of a given size range.

The differential distributions $v(r)$ in Fig. 5, for the initial data from Fig. 1, further demonstrate specific features of particle size distribution over aerosol fractions, previously revealed in terms of the distribution $s(r)$.

It is a common practice in the aerosol microstructure analysis to fit particle size distribution, sampled *in situ*, by a sum of lognormal distributions¹³

$$n(r) = \frac{1}{\sigma r \sqrt{2\pi}} \exp \left[-\left(\ln \frac{r}{r_m} \right)^2 / 2\sigma^2 \right], \quad (4)$$

where r_m is the median radius, and σ is the standard deviation.

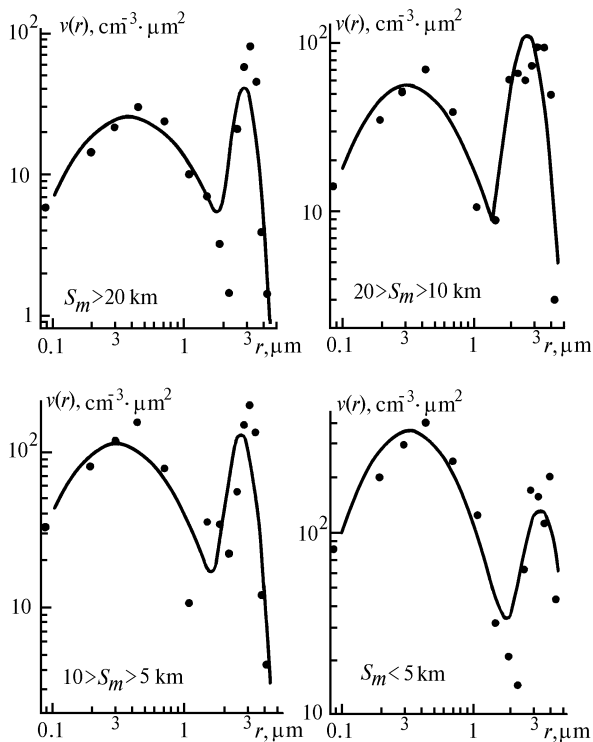


FIG. 5. Particle volume distributions derived by solving the inverse problem (dotts) together with an analytical fit as a sum of lognormal distributions (solid lines).

TABLE I. Integrated microstructure characteristics of winter haze as functions of meteorological visual range (MVR).

MVR, km	N, cm^{-3}	S, km^{-1}	$V, \mu\text{m}^3/\text{cm}^3$	$r_m, \mu\text{m}$	σ
Accumulative fraction					
$S_m > 20$	0.342e3	0.402e-1	0.236e2	0.39	2.32
$10 < S_m < 20$	0.811e3	0.836e-1	0.431e2	0.32	2.15
$5 < S_m < 10$	0.187e4	0.183e00	0.889e2	0.31	2.09
$S_m < 5$	0.475e4	0.510e00	0.283e3	0.33	2.27
Coarse-dispersed fraction					
$S_m > 20$	0.881e00	0.198e-1	0.772e2	2.88	1.17
$10 < S_m < 20$	0.255e01	0.483e-1	0.176e3	2.58	1.25
$5 < S_m < 10$	0.325e01	0.610e-1	0.225e3	2.73	1.20
$S_m < 5$	0.323e01	0.720e-1	0.294e3	3.27	1.29

In a wide range of boundary-layer aerosol models,¹⁰ built up using microphysical data (and shown partly in Fig. 3), the parameter σ is within the range 1.79–2.66 for submicron particles and 1.95–2.74 for particles with $r > 1 \mu\text{m}$.

Therefore, it could be interesting to check the relation (4) applicability to describe results of a solution of the inverse problem. One such an example of fitting the reconstructed distributions $v(r)$ with a sum of two lognormal distributions is illustrated in Fig. 5 by solid lines.

From the figure we see that the reconstructed distributions are fit worst for medium-sized particles, not separated as an individual fraction in this fitting. For distribution $v(r)$, derived by inversion of averages over the complete optical data, the parameter values are found to be $r_{m_1} = 0.32 \mu\text{m}$, $\sigma = 2.27$ for the accumulative mode, and $r_{m_2} = 2.74 \mu\text{m}$, $\sigma = 1.19$ for the coarse mode. Variation of these values with the visual range is obvious from Table I.

From Table I we see that the obtained numerical estimates of σ , the distribution half-width, for winter hazes of various densities are within the typical range of model-derived values in the case of accumulative fraction, and nearly two times lower than the model values for the coarse-fraction. This shows that, according to results of the inverse problem solution, the salient feature of the coarse aerosol fraction of winter season is its narrow distribution.

Also shown in Table I are the estimates of the main integral microstructure characteristics for winter haze aerosols, derived by solving the inverse problem and ordered in the table according to the MVR values. Tabulated parameters of the accumulative fraction are for particles with radii $r > 0.05 \mu\text{m}$. The particle number density in the accumulative fraction is dominated by particles in the size range 0.05–0.15 μm , which, although contributing 75% to the total mass of the fraction, makes no more than 15% of its total geometric cross section. As the atmospheric turbidity grows from the background values ($S_m = 30 \text{ km}$) to an optically dense haze ($S_m = 3 \text{ km}$), the contribution from the accumulative fraction to the total cross section changes nonlinearly from 66% to 88%, as is seen from Fig. 6.

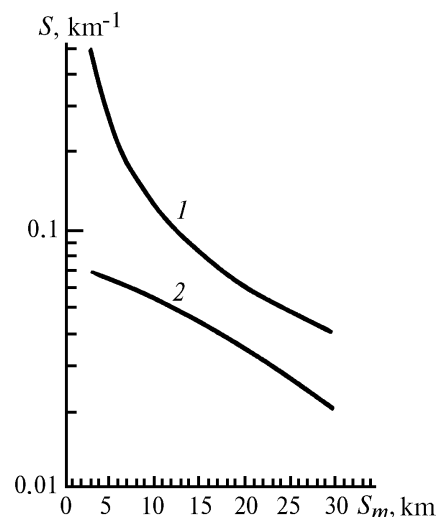


FIG. 6. Total geometric cross section S of aerosol particles as a function of meteorological visual range S_m : accumulative fraction (1) and coarse fraction (2).

The coarse fraction, while contributing only fractions of percent to the number density, contributes to the total particulate volume per cubic cm as much as the accumulative fraction in a strongly turbid atmosphere, and three times more than the accumulative fraction under the background conditions. This emphasizes the need in highly accurate measurements of the concentration of coarse-industrial aerosols to obtain a reliable estimate of their impact on ecological situation.

Summarizing the above said we should like to note that, in the study of optical and microphysical properties of winter haze^{1,3} as a part of the problem of atmospheric aerosol, the specific features of aerosol formation under negative temperatures, when the phase transitions of atmospheric moisture occur, are of primary importance.

With the numerical estimates of microstructure parameters of winter haze aerosol obtained, it is possible to pass from the measured coefficients of aerosol extinction to other optical characteristics, such as elements of scattering matrix, within the limits of their information content being related to the size spectrum.

ACKNOWLEDGMENTS

This work was supported in part by the Russian Foundation for Fundamental Research (grant No. 94-05-16463-a).

REFERENCES

1. V.N. Uzhegov, Yu.A. Pkhalagov, and N.N. Shchelkanov, *Atmos. Oceanic Opt.* **7**, No. 8, 570–574 (1994).
2. Yu.A. Pkhalagov, V.N. Uzhegov, and N.N. Shchelkanov, *Atmos. Oceanic Opt.* **5**, No. 6, 423–426 (1992).
3. E.V. Makienko, Yu.A. Pkhalagov, R.F. Rakhimov, V.N. Uzhegov, and N.N. Shchelkanov, *Atmos. Oceanic Opt.* **7**, No. 12, 816–818 (1994).
4. B.S. Kostin, E.V. Makienko, and I.E. Naats, in: *Problems of Remote Sensing of the Atmosphere* (Institute of Atmospheric Optics, Siberian Branch of the Academy of Sciences of the USSR, Tomsk, 1976), pp. 86–97.
5. I.E. Naats, *Theory of Multifrequency Laser Sensing of the Atmosphere* (Nauka, Novosibirsk, 1980), 157 pp.
6. A.N. Tikhonov and V.Ya. Arsenin, *Methods of Solution of Ill-Posed Inverse Problems* (Nauka, Moscow, 1974), 203 pp.
7. V.E. Zuev and I.E. Naats, *Inverse Problems in Laser Sensing of the Atmosphere* (Nauka, Novosibirsk, 1982), 242 pp.
8. V.V. Veretennikov, *Atm. Opt.* **3**, No. 10, 939–946 (1990).
9. L.S. Ivlev, *Chemical Composition and Structure of Atmospheric Aerosols* (State University, Leningrad, 1982), 366 p.
10. *Aerosols and their Climatic Effects. Report of WMO (CAS) Radiation Commission of IAMAP Meeting of Experts WCP-55*, Williamsburg, Virg. USA, March 1983, 110 pp.
11. G.M. Krekov and R.F. Rakhimov, *Optical Models of Atmospheric Aerosol* (Institute of Atmospheric Optics, Siberian Branch of the Academy of Sciences of the USSR, Tomsk, 1986), 294 pp.
12. V.L. Filippov, V.P. Ivanov, and N.V. Kolobov, *Dynamics of Optical Weather* (State University, Kazan', 1986), 157 pp.
13. V.E. Zuev and M.V. Kabanov, *Modern Problems in Atmospheric Optics, Vol. 4, Optics of Atmospheric Aerosol* (Gidrometeoizdat, Leningrad, 1987), 254 pp.